A Platinum Open Access Journal for Organic Chemistry

Paper

Free to Authors and Readers | DOAJ Seal | *Arkivoc* **2024** (3) 202312083

Modelling of borrowing hydrogen amination reactions of alcohols and amines in NaOH- or KOH-containing media over metal-free ordered mesoporous nitrogenous carbon catalyst

Carlos E. Hernandez-Tamargo,[a] Talla V.R. Mohan,[a] and Parasuraman Selvam[a,b,c*]

[a]National Centre for Catalysis Research and Department of Chemistry, Indian Institute of Technology-Madras, Chennai 600 036, India
[b]International Research Organization for Advanced Science and Technology, Kumamoto University, 2-39-1 Kurokami, Kumamoto 800-8555, Japan
[c]Delaware Energy Institute, University of Delaware, Newark, 221, Academy Street, DE 19716, U.S.A.

Email: selvam@iitm.ac.in

This paper is dedicated in Honour of Professor Graham Hutchings, FRS

Received 09-13-2023 **Accepted Manuscript** 01-18-2024 **Published on line** 01-29-2024

Abstract

The borrowing hydrogen reaction is a one-pot procedure that allows efficient synthesis and functionalization. This type of reaction usually needs transition metals as catalysts. However, recent reports propose the utilization of metal-free, nitrogen-doped mesoporous carbons as effective catalysts. This metal-free strategy needs a strong basic medium, which is provided by alkali ion hydroxides, with KOH enabling the best molecular conversions and NaOH lagging with an inferior performance. We thus employ density functional theory to investigate the role of the alkali ion hydroxide in the borrowing hydrogen reaction to understand the differences between NaOH and KOH when used as basic agents.

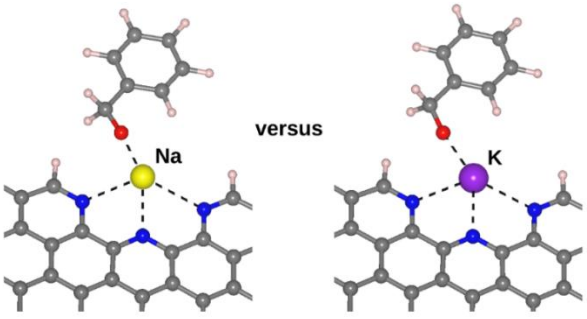

Keywords: Borrowing hydrogen reaction, density functional theory, nitrogen-doped mesoporous carbons.

Introduction

The borrowing hydrogen (BH), or the hydrogen auto-transfer (HAT) amination, is a highly effective method and a one-pot process employed in the synthesis of fine chemicals *via* the formation of C–C, C–O, and C-N bonds using stable and easily accessible substrates such as amines and alcohols.[1] This approach is regarded as one of the most environment-friendly and efficient ways to synthesize intricate amines. The BH principle consists of three general steps: (i) a simpler molecule is dehydrogenated in the presence of a catalyst, (ii) the dehydrogenation product undergoes additional transformations through intermediate reactions, forming a larger compound, (iii) and finally, in the third step, this larger, unsaturated aggregate is hydrogenated.[1] Catalysts are critical in this process since they store the H_2 equivalent transferred from the donor molecule during the initial dehydrogenation step, to be used afterward in the hydrogenation of the product of the intermediate reactions.

In this context, transition metal atoms are considered highly relevant for the successful transfer of the H_2 equivalent.[1–5] On this basis, the potential introduction of carbon materials as novel, metal-free heterogeneous catalysts, is an important step forward, which could further improve the sustainability of the BH method. With this in mind, ordered mesoporous nitrogen-doped or nitrogenous carbons (MNC) have been recently proposed by us as a metal-free catalyst for the reaction between benzyl alcohol-derived compounds and benzylamines *via* a BH pathway (Scheme 1).[6,7]

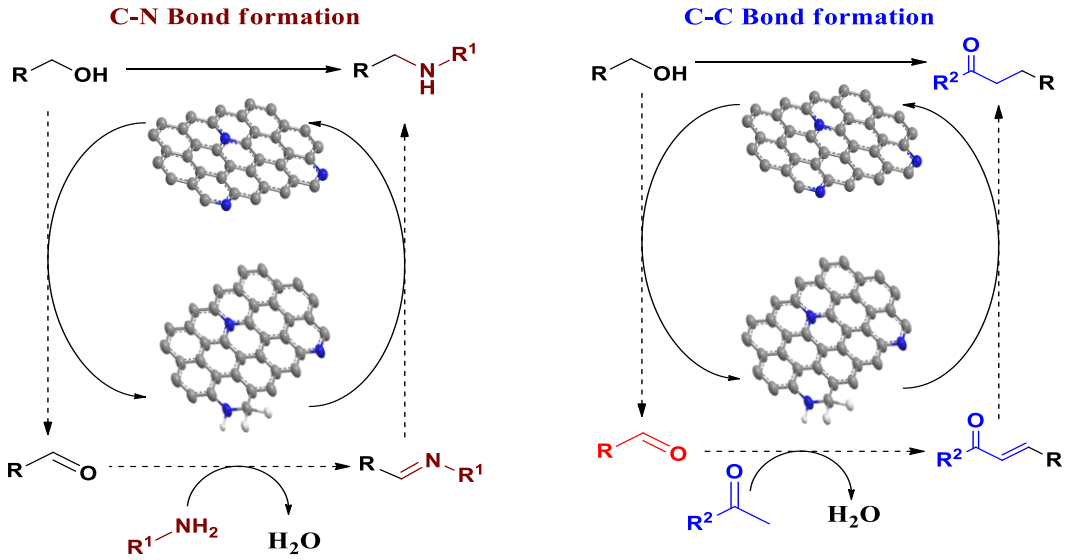

Scheme 1. The B–H reactions established for C–C and C–N bond formation over metal-free nitrogen-doped ordered mesoporous carbonaceous materials. Element colour code: H (white), C (grey), and N (blue).

In our previous work, we synthesized a series of nitrogenous carbons via the nano-casting method, and the characterization and reaction results of the MNC-316 catalyst are shown in Figure 1. It can be seen from Figure 1 that the prepared catalysts exhibit well-ordered mesoporosity as evidenced by powder X-ray diffraction and transmission electron microscopy, respectively. In addition, the elemental analysis showed that we were able to dope nearly 18 wt % of nitrogen into the mesoporous carbon matrix. Furthermore, Figure 1d depicts the X-ray photoelectron spectroscopic which gives the pyridinic and graphitic compositions of the catalyst. Table 1

summarizes the outcome of the C-N coupling reaction performed using the MNC-316, demonstrating an impressive amine yield and exceptional recyclability, as shown in Figure 1c.

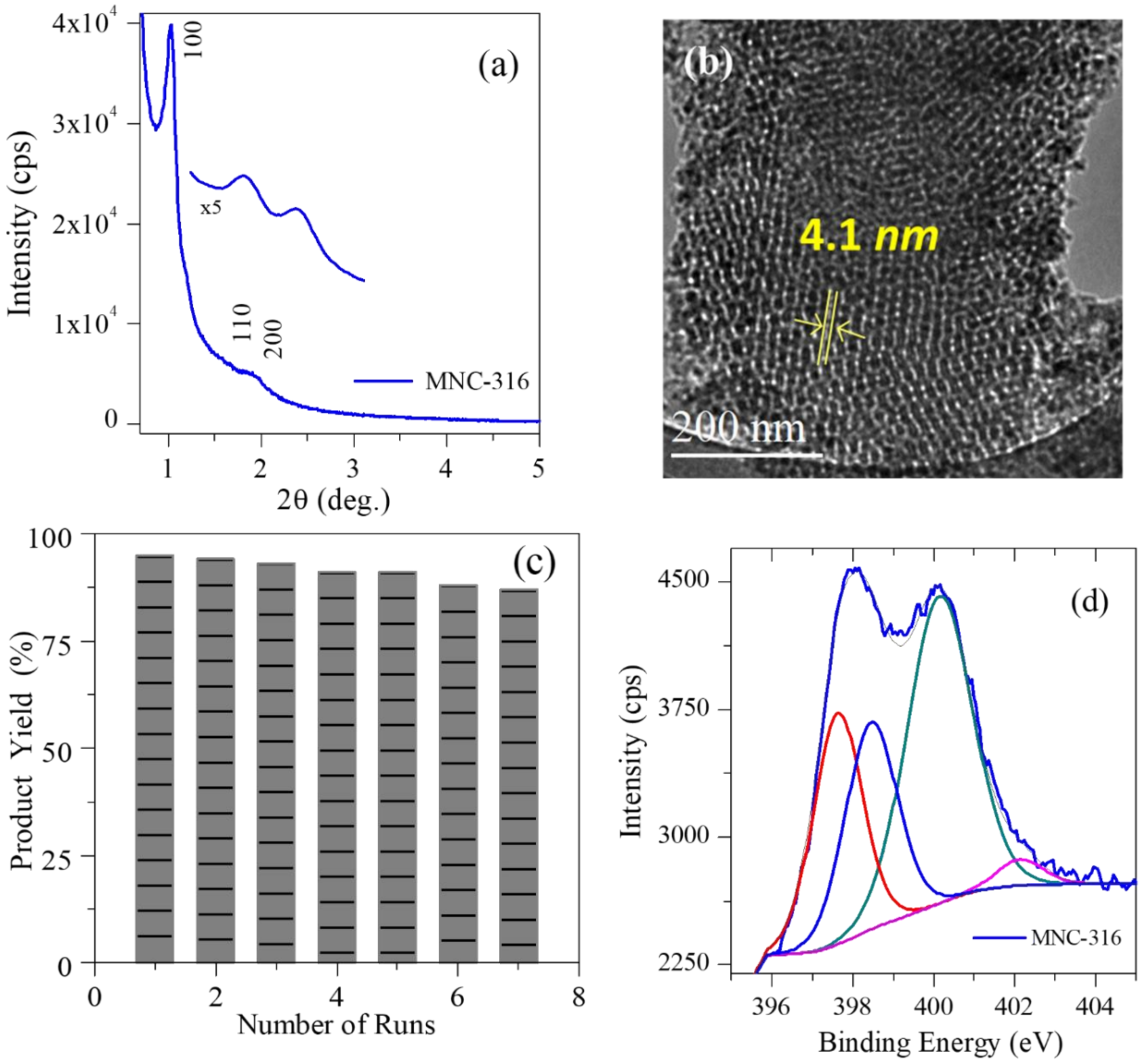

Figure 1. (a) Low Angle XRD patterns and (b) HR-TEM image, of the model catalyst MNC-316; (c) Recyclability tests for the prepared catalyst for the C-N direct amination reaction; (d) High Resolution N (1s) core-level spectra for the prepared catalyst.

Scheme 2 represents the different steps involved in this process.[7] During the first two steps, the benzyl alcohol-derived molecule is dehydrogenated and its OH group is transformed into an aldehyde moiety under alkaline conditions, with the direct participation of the catalyst. A condensation reaction with an amine follows, ending with the hydrogenation of the condensation aggregate. For this kind of reaction, conversions of > 99% were obtained, with almost complete selectivity towards the hydrogenated condensation product (*see Table 1)*.[7] At this juncture, it is important to highlight that nitrogen doping is essential since the undoped carbons were inactive for the same kind of reactions. Experimental evidence pointed to nitrogen atoms at the edge of graphite sheets occupying pyridinic positions (*pyri*-N) as the catalytic active sites. This was justified by the linear increase of the material performance with the content of *pyri*-N. However, other carbon nitrides with a similar layered

structure and higher nitrogen concentration, *e.g.,* g-C_3N_4, did not show catalytic activity, emphasizing the specificity of the MNC materials.[7] Furthermore, density functional theory (DFT) calculations have shown that the presence of potassium hydroxide (KOH) is critical for the catalytic performance of the MNC.[7] After the first dehydrogenation step in Scheme 2; step 1, the organic salt of potassium adsorbs at the edge of the MNC *via* the interaction between potassium and nitrogen, as shown in Figure 2. This potassium-mediated adsorption anchors the molecule near the catalytic active sites and allows the hydrogen transfer from the molecule to the carbon matrix, forming the aldehyde (Scheme 2; step 2). It is important to mention that in pristine carbons, without nitrogen doping, the DFT-calculated adsorption energies are much weaker, thus indicating that only the nitrogen sites can anchor the molecules via the potassium ions.[7]

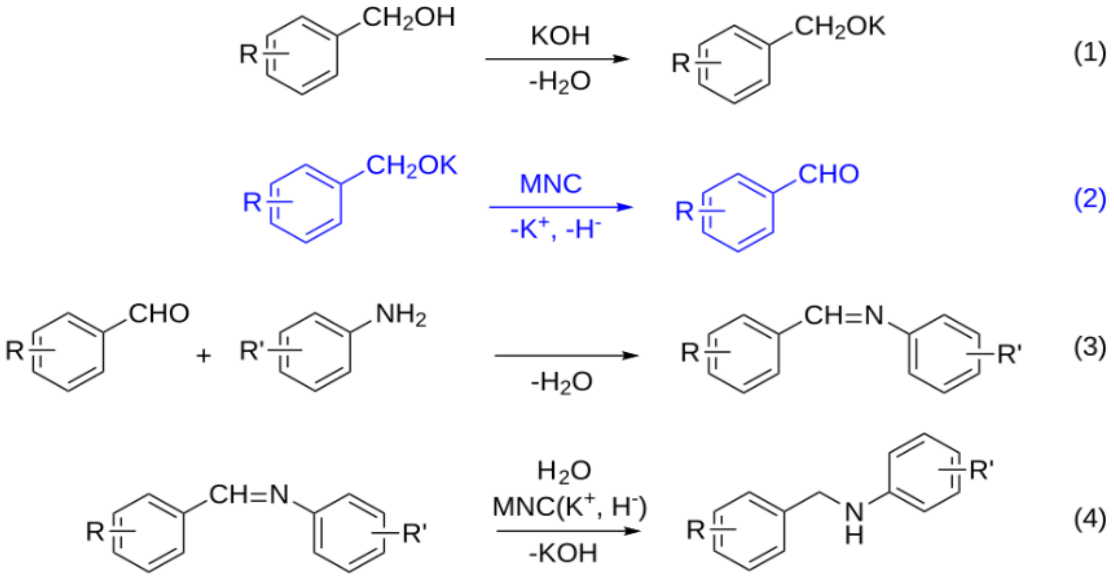

Scheme 2. Reaction steps for the condensation of benzyl alcohol-derived compounds and anilines *via* a borrowing hydrogen pathway.

In the present work, we extend our earlier computational study, aiming to compare the performance of BH amination reaction between alcohols and amines over MNC catalyst in the presence of sodium hydroxide and potassium hydroxide. This is because the reaction occurred with higher efficiency (98%) for the KOH base and lower efficiency for the NaOH base (37%) for both catalyzed and uncatalyzed reactions (*see* Table 1). Since the role of the alkali ion is critical during the adsorption at the edge of the MNC and the formation of the aldehyde, we focus our attention on the second step of the BH reaction represented in Scheme 2
and highlighted in blue.

Results and Discussion

In Table 1, relevant results originally reported by Mohan *et al.* are listed.[7] It is observed that, without either the MNC material or a strongly basic medium, the BH reaction does not take place. Additionally, KOH is a much better additive than NaOH, with alcohol conversions of 99 and 61% and selectivity to the amine of 99 and 60%, respectively. We thus employed DFT calculations to investigate the observed differences between KOH and NaOH during the catalysis of the BH reaction. The overall catalytic process represented in Scheme 2, steps 1 and

2, involves the transfer of two H atoms from benzyl alcohol, with the subsequent formation of benzaldehyde. The edge of the graphene-like sheet is expected to bind H atoms at successive stages of the reaction, with the first H arriving as a hydride H^- ion from the alkali ion benzyloxide thereby forming benzaldehyde (step 2 in Scheme 2), and the second H transferred from water as a proton H^+ in a subsequent step, re-forming the alkali ion hydroxide. A similar mechanism has been proposed for the amination of alcohols in carbon materials, where carbonyl groups are considered the possible active sites.[8]

Table 1. Effect of base concentration for alcohol amination reaction with ordered mesoporous nitrogenous carbon catalyst[a,b,c]

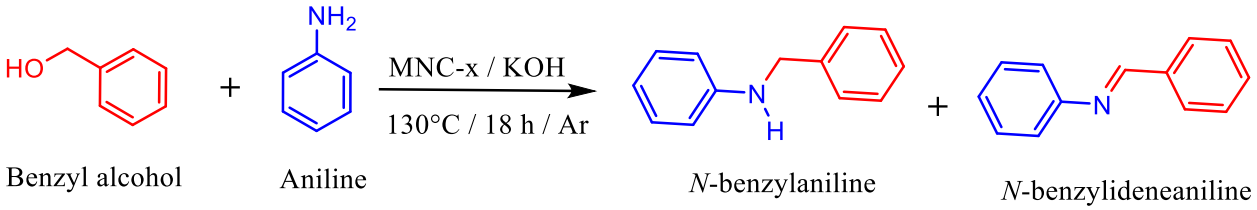

Catalyst	Base	Alcohol conversion (%)	Product distribution (%)	
			Amine	Imine
MNC-316	KOH	> 99	99	1
	NaOH	61	60	1
	No base	0	0	0
No catalyst	KOH	32	13	19
	NaOH	10	3	7

[a] General reaction conditions: Benzyl alcohol (1 mmol); Aniline (1.5 mmol); Base (0.3 Equiv.); Temperature (130°C); Time (18 h); Catalyst (20 wt% of benzyl alcohol); Solvent (toluene, 1 mL); Atmosphere (argon).

[b] Substrate and product selectivity were determined by GC-FID using dodecanol as the external standard. The reactions were repeated two times, and the average results were provided.

[c] Data from Mohan *et al.*[7]

We considered the initial hydride transfer critical (step 2 in Scheme 2), which is initiated with the adsorption of the alkali ion benzyloxide at the edge of the material where the N atoms are located with available lone pairs oriented parallel to the plane of the graphene sheet. We thus calculated the adsorption energies for N-doped carbons represented by a truncated graphite structure with exposed edges terminated by H atoms, with the structures and adsorption energies shown in Figure 2. The calculations indicated that the adsorption energy becomes more favourable with the number of doping N atoms, varying from -100 and -75 kJ/mol for sodium and potassium, respectively, when adsorbed on one N atom, to -211 and -163 kJ/mol when the adsorption takes place on three N atoms. Therefore, the anchoring of the benzyloxide molecule *via* the alkali ion, as the initial requirement for the hydride transfer, is attained at the edge of the N-doped materials. This outcome is consistent with previous experimental and computational reports on N-doped graphene, which highlight the importance of the interaction between potassium and nitrogen to enhance the potassium storage capacities of these materials.[9–12] However, if strong adsorption energy is taken as the magnitude to measure the performance of the alkali hydroxide to co-catalyze the BH reaction, then these results contradict the data listed in Table 1

since NaOH has stronger adsorption energy, albeit with poorer performance in the BH reaction. Nevertheless, we should also consider the kinetic properties of this reaction to establish a better comparison.

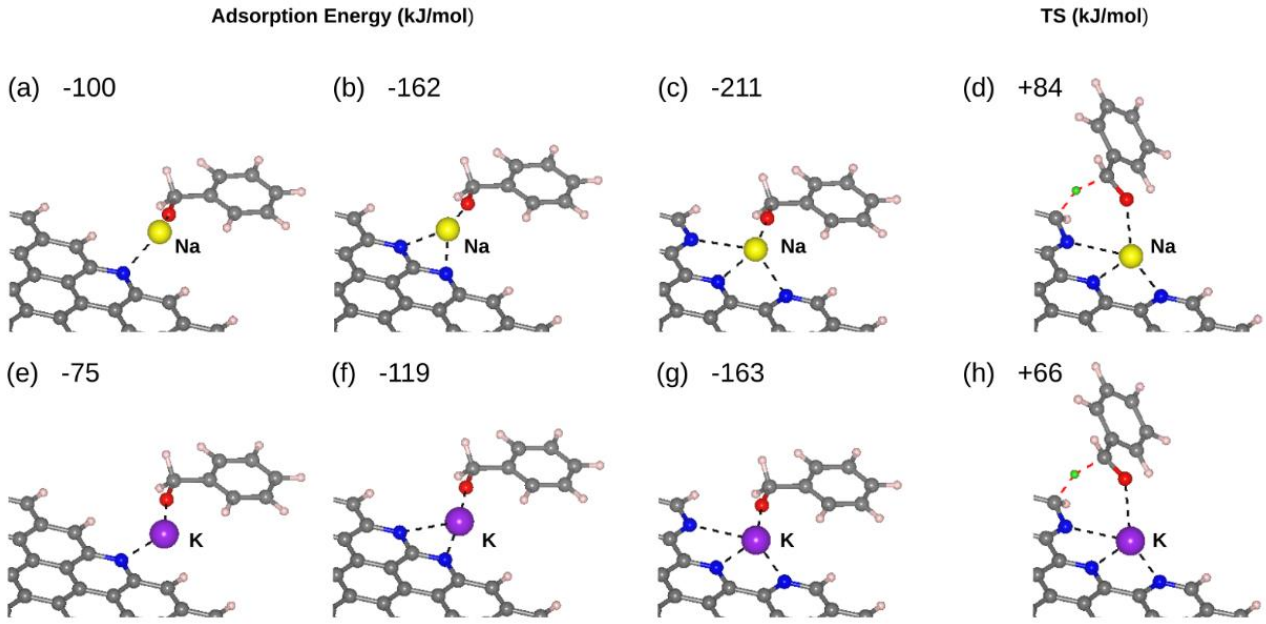

Figure 2. Optimized structures for the adsorption of (a-c) NaOH and (e-g) KOH on N-doped graphite with an increasing number of N atoms; the adsorption energy for each structure is reported in kJ/mol units. Transition states for the transfer of a hydride ion from (d) NaOH and (h) KOH to the nitrogen-doped carbon matrix forming aldehyde. The energy barrier for the transition state is reported for each system in kJ/mol units. Only the carbon layer with the nitrogen doping is shown, deleting the rest of the graphite structure for a better view. Element colour code: H (white), H^- ion in the transition state (green), C (grey), N (blue), O (red), and K (purple).

We also calculated the energy barriers for the transfer of the H^- ion from benzyloxide, leading to the formation of benzaldehyde. We obtain a value of +84 kJ/mol for this transition barrier when sodium benzyloxide is adsorbed at the edge of N-doped graphite, and a value of +66 kJ/mol for potassium benzyloxide, as shown in Figure 2. We can tentatively propose that the adsorption of sodium benzyloxide on the N-doped carbon is very strong, stiffening the structure, and thereby hindering the H^- ion transfer and the continuation of the overall reaction. We could suggest that the adsorption of potassium benzyloxide seems to be more balanced in comparison, sufficiently strong to anchor the benzyloxide molecule to the carbon matrix via the K-N linkage but giving the benzyloxide molecule more freedom of movement compared to the Na-bound case, thereby making it easier for the H^- ion transfer to occur with the consequent formation of the aldehyde. However, a more conclusive explanation will require further analysis, which would determine whether the structural flexibility of the reactant and the transition state is responsible for the lower catalytic performance of NaOH compared to KOH.

Conclusions

In this work, we have presented a density functional theory study on the role of NaOH and KOH as co-catalysts in the borrowing hydrogen reaction. We have specifically analyzed the adsorption of sodium benzyloxide and

potassium benzyloxide on nitrogen-doped graphite, which is considered a critical step that allows the transfer of hydrogen as a hydride ion from the benzyloxide to the carbon matrix forming the aldehyde. It has been experimentally observed that the base KOH is significantly better at facilitating the borrowing hydrogen reaction than NaOH. Based on the preliminary DFT outcomes presented here, we would suggest that the adsorption of sodium benzyloxide on the nitrogen-doped graphite is much stronger than for potassium benzyloxide, which would reduce the freedom of movement of the benzyloxide molecule and the likelihood of the hydride ion to get closer and be transferred to the carbon matrix. This is in principle supported by a higher activation energy for the Na-bound molecule when compared to the potassium case. However, further analysis is required to verify the certainty of this hypothesis.

Experimental Section

Experimental Method

The metal-free ordered mesoporous nitrogen-doped carbon catalyst, *viz.*, MNC-316, was prepared using nano-casting methods, employing an ordered mesoporous silica (SBA-15) hard template as the structure-directing agent and carbon- and nitrogen-rich precursors. Typically, for the preparation of MNC-316, ethylene diamine and carbon tetrachloride are allowed to infiltrate and self-polymerize within the nano-porous space of the template and then subjected to pyrolysis under an argon atmosphere at 600℃. Finally, the silica template was etched out using 5% hydrofluoric acid, thus obtaining the final desired ordered mesoporous nitrogenous carbon catalyst, designated as MNC-316. The prepared catalyst was systematically characterized using various analytical, spectroscopic, and imaging techniques.[7] A detailed account of the synthesis procedure and characterization methods employed for the catalysts is given in the supplementary material.

Computational Methods

Models. The initial step for the preparation of the nitrogen-doped systems used to model the activity of the carbon materials consists of the geometry optimization of the graphite structure. In this case, a 6 × 6 × 2 expansion of the hexagonal unit cell of graphite was employed in the simultaneous optimization of the cell vectors and atomic coordinates (see Figure 3). This 6 × 6 × 2 expansion is needed to make the dimension of the system compatible with the sole utilization of the Gamma point to describe the reciprocal space of the periodic system. The optimized hexagonal unit cell of graphite yields values of 2.470 and 6.741 Å for the vectors a and c, respectively, with a C–C bond length and interlayer distance of 1.426 and 3.370 Å, respectively. These numbers are in good agreement with previously published experimental and computational work.[13,14]

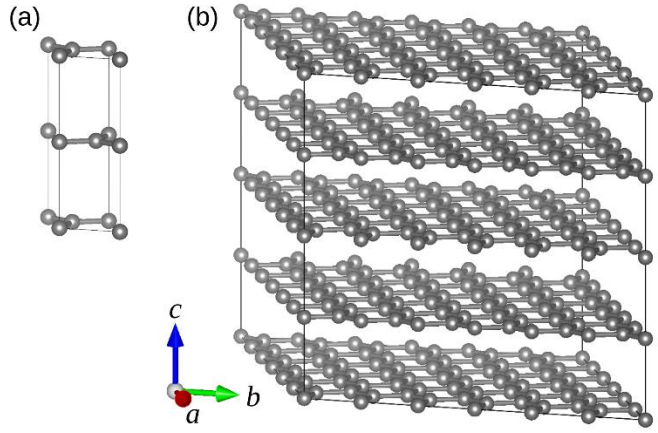

Figure 3. (a) Hexagonal unit cell of graphite. (b) 6 × 6 × 2 expansion of the unit cell of graphite. Element colour code: C (grey).

The simulation cell was prepared following a 6 × 2 × 3 expansion of the orthorhombic unit cell of graphite along the vectors a, b, and c, respectively. The structure is truncated along the vector b, adding a vacuum gap of at least 20 Å to reproduce a material with zig-zag edges; the dangling C–C bonds are saturated with H atoms. This procedure generates a cell with a dimension of 14.8 × 32.3 × 20.2 $Å^3$. The N-doped graphite was constructed by replacing carbon atoms with nitrogen atoms at the edge of the central graphene layer within the orthorhombic cell (see Figure 4). The N-doped graphite, with a variable number of N atoms, was employed to study the adsorption of sodium benzyloxide and potassium benzyloxide and the consequent transfer of the H^- ion from benzyloxide to graphite, forming benzaldehyde.

Calculation parameters. The calculations were performed with the code CP2K employing density functional theory (DFT) within the generalized gradient approximation (GGA).[15,16] Specifically, we used the revised version of the Perdew-Burke-Ernzerhof (rev-PBE) exchange-correlation functional in combination with a non-local correlation functional to approximately account for long-range van der Waals interactions (rVV10).[17–19] The valence states of the atoms were treated with the molecule-optimized basis set DZVP-MOLOPT-SR,[15] while the inner region of the atoms was described with the separable dual-space Goedecker-Teter-Hutter (GTH) pseudopotentials.[20–22] The real-space integration grid employed in the present work was characterized by a cut-off energy for the finest grid of 300 Ry, out of a total of four levels. The mapping of the Gaussian functions onto this multi-grid system was controlled by a reference grid with a cut-off energy of 50 Ry. The cell and geometry optimizations were carried out with the Broyden-Fletcher-Goldfarb-Shanno (BFGS) algorithm,[23] with convergence criteria for the maximum ionic forces and electronic self-consistent iterations of $2×10^{-3}$ Hartree $Bohr^{-1}$ and 10^{-6} Hartree, respectively. Additionally, we made use of the Fermi-Dirac distribution to define the smearing of the electronic states, applying a broadening temperature of 300 K, to improve the convergence of the electronic structure.[24]

We used the improved dimer method (IDM), with a convergence threshold for the ionic forces of $2×10^{-3}$ Hartree×$Bohr^{-1}$, to search for the transition state corresponding to the transfer of the hydride ion from benzyloxide to the N-doped carbon materials. This procedure was applied to the multi-layered graphite system doped with three N atoms.[25] Due to the large number of atoms in the simulation cell, in the vibrational calculation that precedes the IDM calculation, only the layer where alkali ion benzyloxide is adsorbed was allowed to relax, whereas the rest of the material was kept frozen. These constraints were also applied to the IDM calculations.

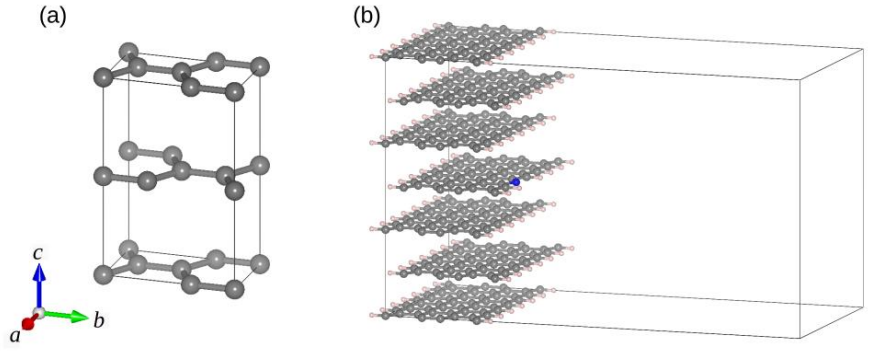

Figure 4. Simulation cells used in the DFT modelling of all-carbon and N-doped graphite (delimited with black lines). (a) The orthorhombic unit cell of all-carbon graphite. (c) 6x2x3 expansion of the N-doped graphite cell with the zig-zag edge exposed. Element colour code: H (white), C (grey), and N (blue).

Acknowledgments

The authors thank the Science and Engineering Research Board (SERB), Department of Science and Technology (DST), New Delhi for funding NCCR, IIT-Madras under grant No. IR/S1/CU-01/2002; Professor B. Viswanathan, Professor Shinya Hayami, and Professor Dionisios Vlachos for their encouragement and support. We are also grateful to Professor Nora H. De Leeuw for inspiration. CEH thanks IIT-Madras for the Visiting Faculty appointment under the Young International Faculty (YIF) Scheme, and TVRM thanks CSIR for fellowship under the NET-SRF scheme.

Supplementary Material

Details of the synthesis procedure and characterization methods are provided. The raw data of the DFT calculations is provided in the supplementary zip file *Raw_Data_DFT.zip* which can be requested from the corresponding author (using the email address on the cover page of this article). This zip file contains the Excel files *Adsorption_Energy.xls* and *Transition_State.xls*, which contain the energy of reactants, transition states, and products used to calculate the adsorption energies and energy barriers shown in Figure 2. These energies are extracted from the CP2K output files *cp2k_job.out*, which are stored in the folders provided within the zip file.

References

1. Corma, A.; Navas, J.; Sabater, M. J. *Chem. Rev*. **2018**, *118*, 1410. https://doi.org/10.1021/acs.chemrev.7b00340
2. Irrgang, T.; Kempe, R. *Chem. Rev*. **2019**, *119*, 2524. https://doi.org/10.1021/acs.chemrev.8b00306
3. Bähn, S.; Imm, S.; Neubert, L.; Zhang, M.; Neumann, H.; Beller, M. *ChemCatChem* **2011**, *3*, 1853. https://doi.org/10.1002/cctc.201100255

4. Reed-Berendt, B. G.; Latham, D. E.; Dambatta, M. B.; Morrill, L. C. *ACS Cent. Sci*. **2021**, *7*, 570. https://doi.org/10.1021/acscentsci.1c00125
5. Podyacheva, E.; Afanasyev, O. I.; Vasilyev, D. V.; Chusov, D. *ACS. Catal*. **2022**, *12*, 7142. https://doi.org/10.1021/acscatal.2c01133
6. Selvam, P.; Sasidharan, M.; Bhat, V. T.; Namitharan, K.; Nallagangula, M.; Kala, K.; Mohan, T. V. R. WO/2020/016908, **2020**.
7. Mohan, T. V. R.; Nallagangula, M.; Kala, K.; Hernandez-Tamargo, C. E.; De Leeuw, N. H.; Namitharan, K.; Bhat, V. T.; Sasidharan, M.; Selvam, P. *J. Catal*. **2023**, *419*, 80. https://doi.org/10.1016/j.jcat.2023.02.005
8. Yang, H.; Cui, X.; Dai, X.; Deng, Y.; Shi, F. *Nat. Commun*. **2015**, *6*, 6478. https://doi.org/10.1038/ncomms7478
9. Share, K.; Cohn, A. P.; Carter, R.; Rogers, B.; Pint, C. L. *ACS Nano* **2016**, *10*, 9738. https://doi.org/10.1021/acsnano.6b05998
10. Hassan, F. M.; Chabot, V.; Li, J.; Kim, B. K.; Ricardez-Sandoval, L.; Yu, A. *J. Mater. Chem. A Mater*. **2013**, *1*, 2904. https://doi.org/10.1039/c2ta01064j
11. Ju, Z.; Li, P.; Ma, G.; Xing, Z.; Zhuang, Q.; Qian, Y. *Energy Storage Mater*. **2018**, *11*, 38. https://doi.org/10.1016/j.ensm.2017.09.009
12. Chen, P.; Yang, J.-J.; Li, S.-S.; Wang, Z.; Xiao, T.-Y.; Qian, Y.-H.; Yu, S.-H. *Nano Energy* **2013**, *2*, 249. https://doi.org/10.1016/j.nanoen.2012.09.003
13. Trucano, P.; Chen, R. *Nature* **1975**, *258*, 136. https://doi.org/10.1038/258136a0
14. Avramov, P. V.; Sakai, S.; Entani, S.; Matsumoto, Y.; Naramoto, H. *Chem. Phys. Lett*. **2011**, *508*, 86. https://doi.org/10.1016/j.cplett.2011.04.016
15. Kühne, T. D.; Iannuzzi, M.; Del Ben, M.; Rybkin, V. V.; Seewald, P.; Stein, F.; Laino, T.; Khaliullin, R. Z.; Schütt, O.; Schiffmann, F.; Golze, D.; Wilhelm, J.; Chulkov, S.; Bani-Hashemian, M. H.; Weber, V.; Borštnik, U.; Taillefumier, M.; Jakobovits, A. S.; Lazzaro, A.; Pabst, H.; Müller, T.; Schade, R.; Guidon, M.; Andermatt, S.; Holmberg, N.; Schenter, G. K.; Hehn, A.; Bussy, A.; Belleflamme, F.; Tabacchi, G.; Glöß, A.; Lass, M.; Bethune, I.; Mundy, C. J.; Plessl, C.; Watkins, M.; VandeVondele, J.; Krack, M.; Hutter, J. *J. Chem. Phys*. **2020**, *152*, 194103. https://doi.org/10.1063/5.0007045
16. R. G. Parr and W. Yang, *Density Functional Theory of Atoms and Molecules*; Oxford University Press, 1989.
17. Perdew, J. P.; Burke, K.; Ernzerhof, M. *Phys. Rev. Lett*. **1996**, *77*, 3865. https://doi.org/10.1103/PhysRevLett.77.3865
18. Zhang, Y.; Yang, W. *Phys. Rev. Lett*. **1998**, *80*, 890. https://doi.org/10.1103/PhysRevLett.80.890
19. Sabatini, R.; Gorni, T.; de Gironcoli, S. *Phys. Rev. B*. **2013**, *87*, 041108. https://doi.org/10.1103/PhysRevB.87.041108
20. Hartwigsen, C.; Goedecker, S.; Hutter, J. *Phys. Rev. B*. **1998**, *58*, 3641. https://doi.org/10.1103/PhysRevB.58.3641
21. Goedecker, S.; Teter, M.; Hutter, J. *Phys. Rev. B*. **1996**, *54*, 1703. https://doi.org/10.1103/PhysRevB.54.1703
22. Krack, M. *Theor. Chem. Acc*. **2005**, *114*, 145. https://doi.org/10.1007/s00214-005-0655-y

23. R. Fletcher, *Practical Methods of Optimization*; 2nd ed. ; New York : John Wiley & Sons, 1987.
24. Mermin, N. D. *Physical Review* **1965**, *137*, A1441. https://doi.org/10.1103/PhysRev.137.A1441
25. Heyden, A.; Bell, A. T.; Keil, F. J. *J. Chem. Phys*. **2005**, *123*, 224101. https://doi.org/10.1063/1.2104507